American Mineralogist, Volume 92, pages 1303–1315, 2007

Laser Raman microspectrometry of metamorphic quartz: A simple method for comparison of metamorphic pressures

Masaki Enami,[1,*] Tadao Nishiyama,[2] and Takashi Mouri[1]

[1]Department of Earth and Planetary Sciences, Nagoya University, Chikusa-ku, Nagoya 464-8602, Japan
[2]Department of Earth and Environment, Kumamoto University, 2-39-1 Kurokami, Kumamoto 860-8555, Japan

Abstract

A Laser Raman microspectrometry method was applied to metamorphic quartz in quartz-eclogite-, epidote-amphibolite-, and amphibolite-facies rocks to assess the quantitative correlation between the Raman frequency shift and metamorphic pressure. Quartz crystals sealed in garnet and other phases have a higher frequency shift than those in the matrix. Furthermore, the quartz inclusions show a frequency shift specific to the individual host crystals in eclogites (garnet ≈ kyanite > omphacite ≈ epidote). These observations imply that the residual pressures retained by quartz inclusions depend on elastic parameters of the host crystals, as discussed by previous researchers. The Raman frequency shift of quartz inclusions in garnet systematically increases with increasing peak metamorphic pressures from the amphibolite facies (0.30–0.55 GPa/470–570 °C), through the epidote-amphibolite facies (0.8–1.1 GPa/470–635 °C) to the quartz-eclogite facies (2.1–2.5 GPa/660–710 °C). Calibrations based on experimental work suggest that the measured Raman frequency shifts signify residual pressures of 0.1–0.2, 0.4–0.6, and 0.8–1.0 GPa for these three groups of metamorphic rocks, respectively. Normal stresses (internal pressures) of quartz inclusions in garnet, numerically simulated with an elastic model, and inferred pressure-temperature conditions at peak metamorphic stage are compatible with the residual pressures estimated from the frequency shifts. Laser Raman microspectroscopic analysis of quartz is a simple and effective method for (1) comparison of pressure conditions in metamorphic rocks formed under various pressure-temperature conditions, and (2) detection of a higher-pressure signature in metamorphic rocks extensively recrystallized during the subsequent exhumation and hydration stage.

Keywords: Raman shift, quartz, residual pressure, metamorphism, elastic model

Introduction

Laser Raman microspectroscopy is a useful tool for identification of minute crystals in terrestrial and extraterrestrial materials and inclusions in optically transmissive host phases (e.g., Wang et al. 1999; Gillet et al. 2002; Zedgenizov et al. 2004). The Raman spectral investigations of metamorphic rocks have (1) shown that garnet and zircon are useful pressure containers for the preservation of ultrahigh-pressure (UHP) phases (e.g., Sobolev and Shatsky 1990; Sobolev et al. 1995); and (2) revealed evidence for UHP metamorphism such as coesite and microdiamond inclusions in zircon and garnet from extensively retrograded gneissic rocks in several UHP metamorphic terranes (e.g., Tabata et al. 1998; Parkinson and Katayama 1999; Ye et al. 2000; Liu et al. 2001).

Coesite is identified by its diagnostic Raman spectrum with a strong band at about 521 cm^{-1} at room temperature and atmospheric pressure (Sharma et al. 1981; Boyer et al. 1985; Hemley 1987). The main bands of α-quartz are located at about 464, 205, and 128 cm^{-1}. These Raman spectra often show shifts to higher frequency in various degrees depending on their mode of occurrence. Parkinson and Katayama (1999) and Parkinson (2000) reported that (1) the 521 cm^{-1} band of monocrystalline coesite inclusions in unfractured zircon and garnet of Kokchetav UHP metamorphic rocks shifts to 525–526 cm^{-1}; and (2) coesite inclusions occurring inside fractured host crystals show no significant Raman frequency shift. They deduced that the monocrystalline coesite inclusions having the higher Raman frequency shift still retain ultrahigh overpressures (1.9–2.3 GPa).

Ye et al. (2001) classified the coesite/quartz inclusions in zircons from the Dabieshan-SuLu UHP metamorphic terrane into the following three types on the basis of textures: (1) single grains or aggregates of coesite with polycrystalline quartz totally enclosed in zircon without fractures; (2) single crystals or aggregates of coesite with quartz that was exposed on the surface of the section during polishing—these were also enclosed in zircon; and (3) aggregates of coesite and quartz enclosed in zircon with fractures. Ye et al. (2001) showed that the Raman spectra of the coesite and subsidiary quartz inclusions have shifted, and the amount of shifting was closely correlated with the extent to which coesite had been converted to quartz. Shifts in the Raman spectra revealed the following characteristics in the first type of coesite/quartz inclusions: (1) each coesite/quartz inclusion has a

* E-mail: enami@eps.nagoya-u.ac.jp

distinct overpressure, and quartz inclusions tend to retain lower overpressure than coesite inclusions; and (2) monocrystalline quartz inclusions give smaller shifts of Raman spectra (lower overpressures) than polycrystalline quartz inclusions.

Recently, several new applications of the Raman shift for paleo-geobarometry have been proposed. Izraeli et al. (1999) reported an internal pressure of 0.13–0.65 GPa in olivine included in diamond, and calculated source pressures of 4.4–5.2 GPa for Siberian diamonds considering bulk moduli and thermal expansion of these two phases. Sobolev et al. (2000) proposed a "coesite-in diamond" geobarometer that is virtually independent of temperature, and estimated an initial pressure of 5.5 GPa for Venezuela diamond formation. Yamamoto et al. (2002) applied Raman spectroscopic analysis to CO_2-dominated fluid inclusions in mantle-derived xenoliths and estimated residual pressures as 0.96–1.04 GPa. They additionally suggested that the inclusions show pressures specific to the individual host minerals of spinel, orthopyroxene, clinopyroxene, and olivine, similar to the case of our eclogite samples.

In this contribution, we report systematic measurements of Raman spectra of quartz crystals in metamorphic rocks recrystallized under quartz-eclogite-, epidote-amphibolite-, and amphibolite-facies conditions. The primary purposes of our study were to correlate the degree of the frequency shift of quartz crystals with (1) their modes of occurrence; (2) physical properties of the host crystals; and (3) metamorphic pressure/temperature (*P-T*) conditions of their host rocks. Our results show that the Raman frequency shift is a powerful and effective tool to (1) estimate residual pressures retained by minerals; and (2) compare peak pressure that the metamorphic rocks have experienced.

Outline of geology and sample descriptions

Laser Raman microspectroscopic analyses were performed on three *P-T* types of metamorphic rocks: (1) quartz-eclogite; (2) metapelite, metachert, and metabasite of the epidote-amphibolite-facies from the Sanbagawa metamorphic belt in central Shikoku, Japan (Fig. 1; Banno and Nakajima 1992; Takasu et al. 1994); and (3) metapelite of the amphibolite facies from the Altai metamorphic belt in northwestern China (Windley et al. 2002; Zheng et al. 2005). Sample descriptions and representative data set of mineral compositions are given in the Appendix 1.

Sanbagawa metamorphic rocks

The metamorphic conditions of the Sanbagawa belt can be discussed in terms of four mineral zones based on mineral parageneses of metapelites: chlorite, garnet, albite-biotite, and oligoclase-biotite zones in ascending order of metamorphic grade, (Fig. 1a; Enami 1983; Higashino 1990). The metamorphic grades of the albite-biotite and oligoclase-biotite zones are equivalent to those of the epidote-amphibolite facies (Enami et al. 1994). The higher-grade areas in the Besshi region of central Shikoku are subdivided into the eclogite unit, which is the highest structural level of the Sanbagawa belt, and non-eclogite unit (Fig. 1b; Wallis and Aoya 2000), although the exact position of the tectonic boundary between the two units is still uncertain. The eclogite assemblages sporadically occur in the presumed eclogite unit, and are attributed to crystallization in a deeper part of the Sanbagawa subduction zone (Takasu 1989; Ota et al. 2004). Lithologies of the eclogite unit and of the surrounding non-eclogite unit were partially recrystallized under the epidote-amphibolite-facies conditions during the exhumation and hydration stage (Aoya 2001; Zaw Win Ko et al. 2005).

Quartz-eclogite facies rocks

The SiO_2 polymorph presumed to have been stable at peak pressures in the Sanbagawa eclogitic rocks was quartz, not coesite (e.g., Tsujimori et al. 2000; Aoya 2001; Ota et al. 2004). The eclogites examined for Raman barometry were collected from the eclogite unit in the Besshi region (Fig. 1b), and grouped into quartz-rich (QE9601 and GO01TT) and quartz-poor (WK1304 and WK1310) types. Their protoliths are inferred to be sedimentary mixtures of quartzofeldspathic and basaltic materials for the quartz-rich eclogite, and basalt and/or gabbro for the quartz-poor eclogite (Banno et al. 1976; Takasu 1989). In these eclogites, garnet shows a complex zonal structure consisting of a core overgrown by a discontinuous, narrow mantle (50–200 μm in width), which are interpreted to have formed at the eclogite and the later epidote-amphibolite facies stages, respectively. Quartz is included in the garnet core, but could not be found in the mantle. The eclogite geothermobarometer (Krogh Ravna and Terry 2004) gives equilibrium conditions of 2.4 GPa and 680 °C for the quartz-rich eclogite, and 2.1–2.2 GPa and 660–690 °C for the quartz-poor eclogites at the peak metamorphic stage. Equilibrium *P-T* conditions of 2.4–2.5 GPa and 665–710 °C were estimated for kyanite-quartz eclogites collected from the same area as the quartz-rich eclogites that we studied (A. Miyamoto, personal communication). Ota et al. (2004) reported *T* ranging from 510 to 790 °C and *P* from 1.4 to 2.5 GPa for the eclogite assemblages, and attribute the wide range to a *P-T* gradient in the eclogite unit. The equilibrium conditions of the present samples are estimated to correspond to the upper end of the *P-T* range reported by Ota et al. (2004).

Epidote-amphibolite facies rocks

Two metapelites (AS1919 and AS2006) and a metachert (ST22F04b) were collected from the albite-biotite zone of the Asemi-gawa (River Asemi) area (Higashino 1990; Otsuki and Banno 1990) and Saruta-gawa area (Kurata and Banno 1974; Banno 2000) in the inferred non-eclogite unit, respectively (Fig. 1a). The equilibrium conditions of the albite-biotite zone were estimated at 0.8–1.0 GPa and 470–590 °C (Enami et al. 1994; Wallis et al. 2000). The garnet-biotite geothermometer gives an equilibrium temperature of 575 ± 25 °C at 1.0 GPa for AS2006 (Program GTB: http://ees2.geo.rpi.edu/MetaPetaRen/Software/GTB_Prog/GTB.html). A metabasite (AS0305) was sampled from the oligoclase-biotite zone along the Asemi-gawa area. The sample contains no mineral assemblages suitable for the conventional calculations of metamorphic *P-T* conditions. The equilibrium *P-T* conditions of the oligoclase-biotite zone were estimated as 0.9–1.1 GPa/585–635 °C in the Besshi region (Enami et al. 1994; Wallis et al. 2000), and those of the sample studied here are probably within this range.

Altai metamorphic rocks

Late Permian metamorphic rocks from the greenschist to amphibolite facies are widely distributed in the Altai meta-

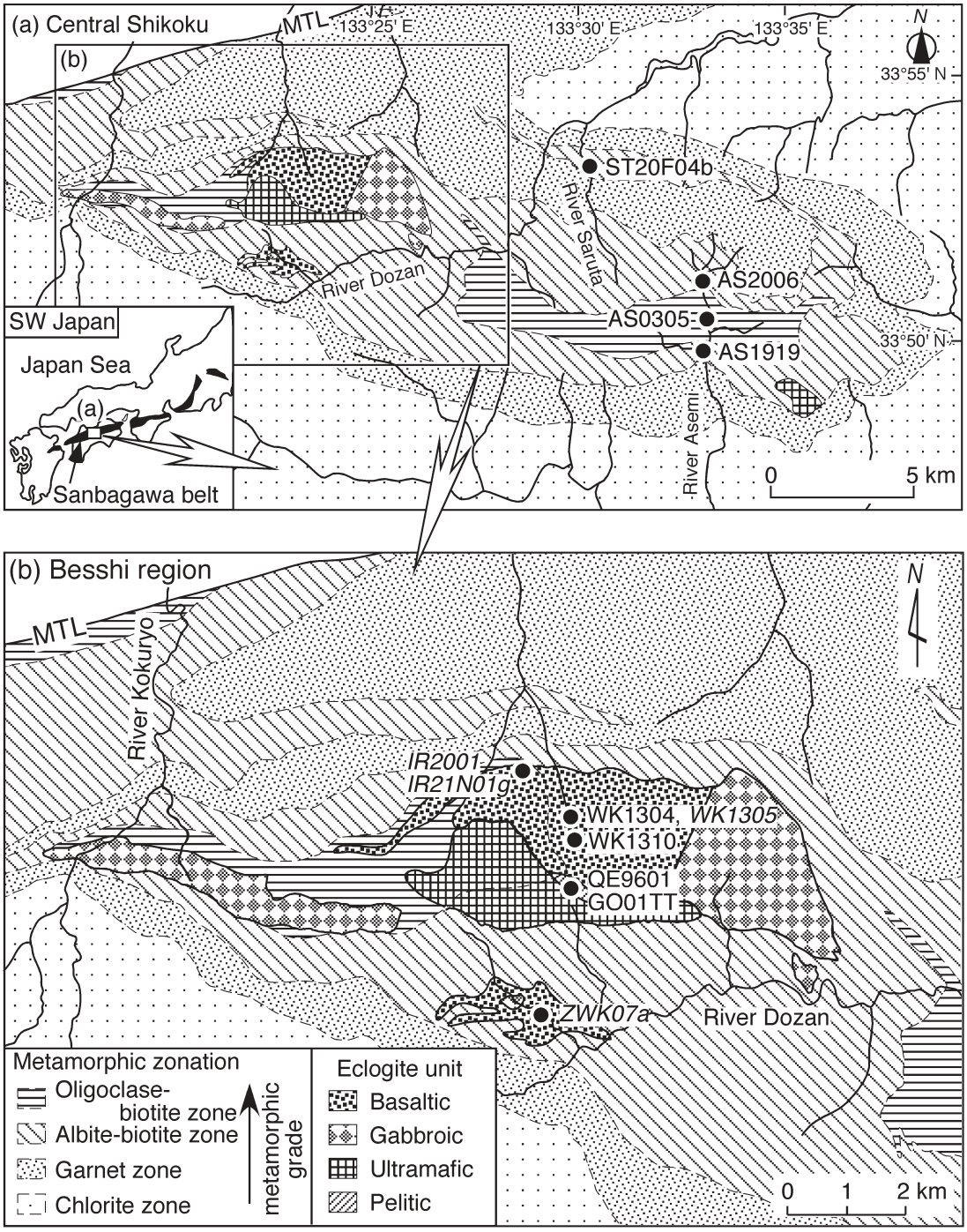

FIGURE 1. Metamorphic zone maps of the Sanbagawa metamorphic belt in central Shikoku (**a**, after Higashino 1990) and the Besshi region (**b**, partly modified from Fig. 1 of Aoya 2001) with sample localities (solid circles). Samples with numbers given in regular font were used to compare Raman frequency shifts with metamorphic pressures (Figs. 6 and 7). Samples with numbers given in italics were used to test the suitability of Raman barometry for recognizing signatures of higher pressure conditions in metamorphic rocks recrystallized during the subsequent exhumation and hydration (Fig. 12).

morphic belt. All three Al_2SiO_5 polymorphs occur in this belt (Windley et al. 2002; Zheng et al. 2005), implying conditions of the medium *P*/*T*-type metamorphic facies series. Conditions for the assemblages of garnet + biotite + muscovite + aluminum silicates + quartz ± plagioclase are estimated to be 0.30–0.55 GPa and 470–500 °C for sample 148-2, and 0.35–0.55 GPa and 520–570 °C for sample 104-9 [Program GTB, THERMOCALC v3.25 and AX (Holland and Powell 1998)], which are close to

those for the Al_2SiO_5 triple point of 0.45 ± 0.05 GPa and 550 ± 50 °C (Pattison 1992).

Laser Raman microspectroscopy and Raman shift

Analytical procedures and spectrographic characterization

Raman spectra were obtained with a laser Raman micro-spectrophotometer, Nicolet Almega XR (Thermo Electron Corp.: gratings 2400 lines/mm), at the Petrology Laboratory of Nagoya University, equipped with a 532 nm Nd-YAG laser, charge-coupled-device (CCD) detector (Andro Technology: 256 × 1024 pixels, cooled by a Peltier element) and an automated confocal microscope (Olympus BX51). The objective is an Olympus Mplan-BD 100X (numerical aperture 0.9). Room temperature was kept at 22 ± 1 °C. Spatial resolution is about 1 μm, and the output power of 25 mW produces an irradiation power of 10 mW on the samples (R. Harui, personal communication). The pinhole diameter is 25 μm and the corresponding spectral resolution is about ~2.5 cm^{-1}. Raman spectra were collected in 6 accumulations of 10 s each. Frequencies of the Raman bands were calibrated by monitoring the position of a plasma line from the Ne laser (703.241 nm). Using the 520 cm^{-1} band of the Si wafer, the analytical reproducibility was checked every day that the analyses were carried out; it was found to be ±0.3 cm^{-1} (1σ level) over two years.

A (0001) section cut from a euhedral crystal of pegmatitic α-quartz was used as a standard. At atmosphere pressure and room temperature, the main band for the α-quartz, which is related to bending vibrations of the intra-tetrahedral O-Si-O angles (Etchepare et al. 1974), is located at about 464 cm^{-1} with subsidiary bands of 128 and 205, 355, and 394 cm^{-1} (Fig. 2). The standard deviation for over 300 duplicate measurements of the wavenumber of α-quartz is less than ±0.04 cm^{-1} for the 464 and 128 cm^{-1} bands and ±0.3 cm^{-1} for the 205 cm^{-1} band (Appendix 2 Fig. 1). The extent of frequency shift of Raman spectra is defined by two parameters, $\omega_1 = \nu_{464} - \nu_{205}$ and $\omega_2 = \nu_{205} - \nu_{128}$, where ν_i denotes wavenumber for each band (Fig. 2). We chose to use differences to avoid systematic errors in measurements of individual ν_i. The standard deviation of ω_1 and ω_2 for the α-quartz standard is ±0.3 cm^{-1}; this level of precision is largely due to the uncertainty in the ν_{205} measurement. Temperature dependencies of ω_1 and ω_2 are estimated as about –0.06 cm^{-1}/°C (Schmidt and Ziemann 2000) and –0.03 cm^{-1}/°C (Dean et al. 1982) at room temperature and 0.1 MPa. The experimentally estimated temperature dependencies of ω_1 and ω_2 are an order-of-magnitude smaller than the measured standard deviations of ω_1 and ω_2 (±0.3 cm^{-1}). Thus a room temperature fluctuation of ±1 °C probably has less influence on the Raman parameters than other factors (Appendix 2 Fig. 1).

The residual pressure retained by quartz inclusions is measured as a function of the difference in ω_1 and ω_2 between the α-quartz standard and the sample: $\Delta\omega_1 = \omega_1^{standard} - \omega_1^{sample}$ and $\Delta\omega_2 = \omega_2^{sample} - \omega_2^{standard}$. These two parameters increase with increasing residual pressure. Most analyzed samples were conventionally polished thin sections 30–50 μm in thickness. Quartz inclusions in a thicker section (80–100 μm in thickness) of a quartz-rich eclogite were additionally analyzed for comparison; this section gave frequency shifts similar to those obtained from sections of standard thickness.

Mode of occurrences of quartz and Raman shift

Quartz occurs as a matrix phase and/or as an inclusion in garnet and other constituent minerals. The quartz inclusions are monocrystalline and mostly 5–20 μm in size. They are usually spherical or ellipsoidal in form (Figs. 3a and 3b), and in some cases anhedral or irregular in shape (Figs. 3c and 3d). Following Ye et al. (2001), we have identified three types of quartz inclusions based on their mode of occurrence. The first type of inclusion is completely surrounded by the host crystal (denoted as Cs = completely surrounded: Fig. 4a). This type of inclusion was carefully checked by depth-step scan analysis with the laser Raman microspectrometer to be sure that it was completely enclosed in the host crystal and was neither touching the glass slide nor exposed on the polished surface. The inclusions were found to be from 5 to 10 μm below the surface in most cases. The second type of inclusion is either partly exposed on the polished surface of host crystal or touches the glass slide (Ex = exposed: Fig. 4b). No fracture is developed in the two types of inclusions and surrounding host crystals, and thus these inclusions were definitely encapsulated in their host crystals during the exhumation stage. The third type of inclusion occurs in a fractured host crystal in which cracks extend from inside the host to the inclusion or into and through the inclusion (Fc = in a fractured host: Figs. 3b and 4c).

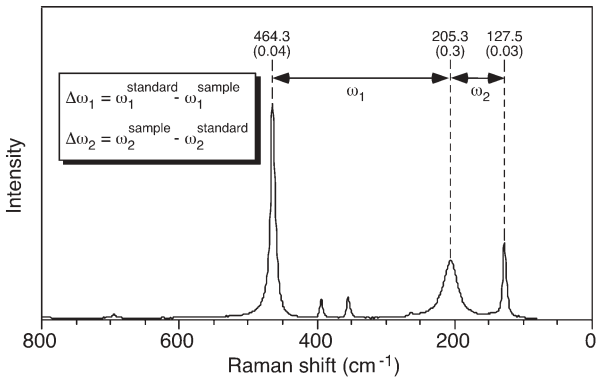

Figure 2. Representative Raman spectrum of α-quartz at atmosphere pressure and room temperature, showing definitions of Raman frequency shifts. Number in parentheses indicates standard deviation (1σ level).

Figures 5a and 5b show a depth-step analysis of a Cs inclusion and a horizontal-step analysis of an Ex inclusion in garnet, respectively. Local increases of the frequency shift of quartz in the narrow domain extending to 2–4 μm from the quartz-garnet interface suggest that the mechanical stress concentrates at this zone, a phenomenon much discussed in the field of material science (e.g., Ito et al. 1994; De Wolf 2003). To avoid the grain-boundary effect on the frequency shift, we will refer only to analytical data from the central part of crystals.

The quartz inclusions in garnets show systematic variations of the frequency shifts depending on their mode of occurrence that are similar to the Raman shift of coesite inclusions in zircon and garnet reported by Parkinson and Katayama (1999), Parkinson (2000), and Ye et al. (2000). The shift in frequency for quartz inclusions in garnet increases in the order Fc, Ex, and Cs (Table 1 and Figs. 6, 7, and 8). The Fc quartz inclusions in garnet and matrix quartz of these samples show the Raman spectra close to those of the α-quartz standard. Most fractures in garnet around the Fc inclusions are likely to have been formed by deformation during subduction and/or exhumation of the metamorphic rocks. Thus the Raman spectra of the Fc inclusions in garnet may express the release of compressive stress (pressure) and subsequent annealing during the exhumation stage. The Ex inclusions in garnet probably record the release of compressive stress in the process of making thin sections. The Cs inclusions are completely sealed in the host crystals, and thus hold more certain information about metamorphic conditions than do the Ex and Fc inclusions in garnet.

In contrast to the case of quartz inclusions in garnet, the Cs quartz inclusions in staurolite have negative and lower $\Delta\omega_1$ (–0.9 ± 0.6 cm^{-1}) and $\Delta\omega_2$ (–0.7 ± 0.7 cm^{-1}) values than the Ex

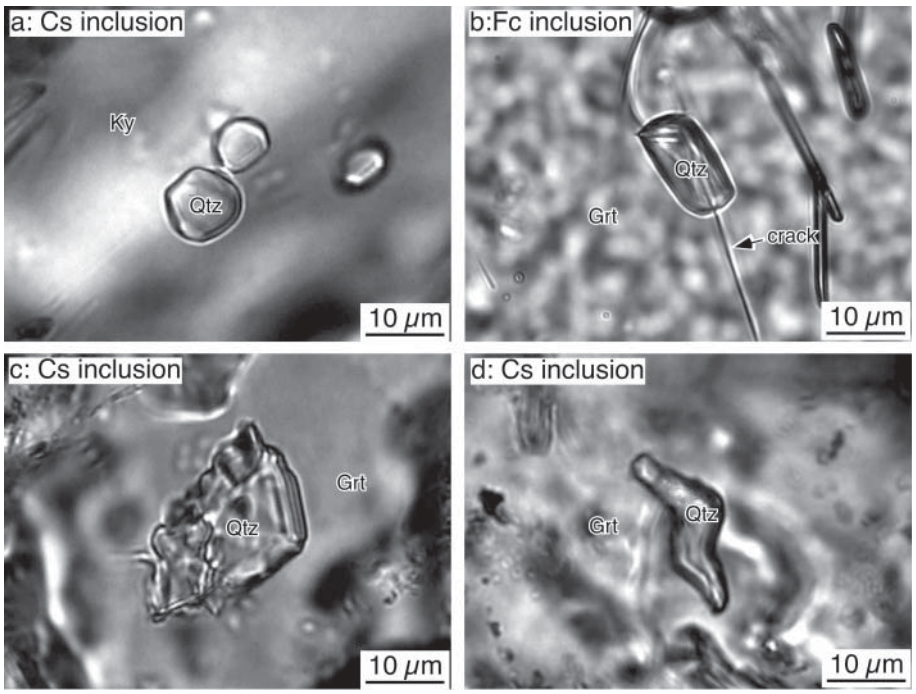

FIGURE 3. Photomicrographs of quartz inclusions in kyanite (**a**) and garnet (**b**, **c**, and **d**) from QE9601 (**a** and **c**), GO01TT (**b**), and AS2006 (**d**). Abbreviations are listed in Table 1.

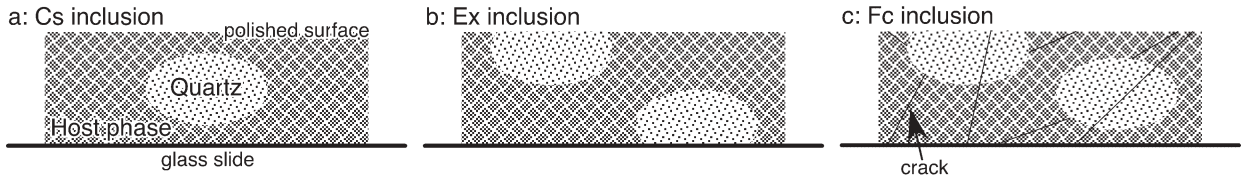

FIGURE 4. Schematic sections of analyzed samples showing three modes of occurrence of quartz inclusions in a host phase.

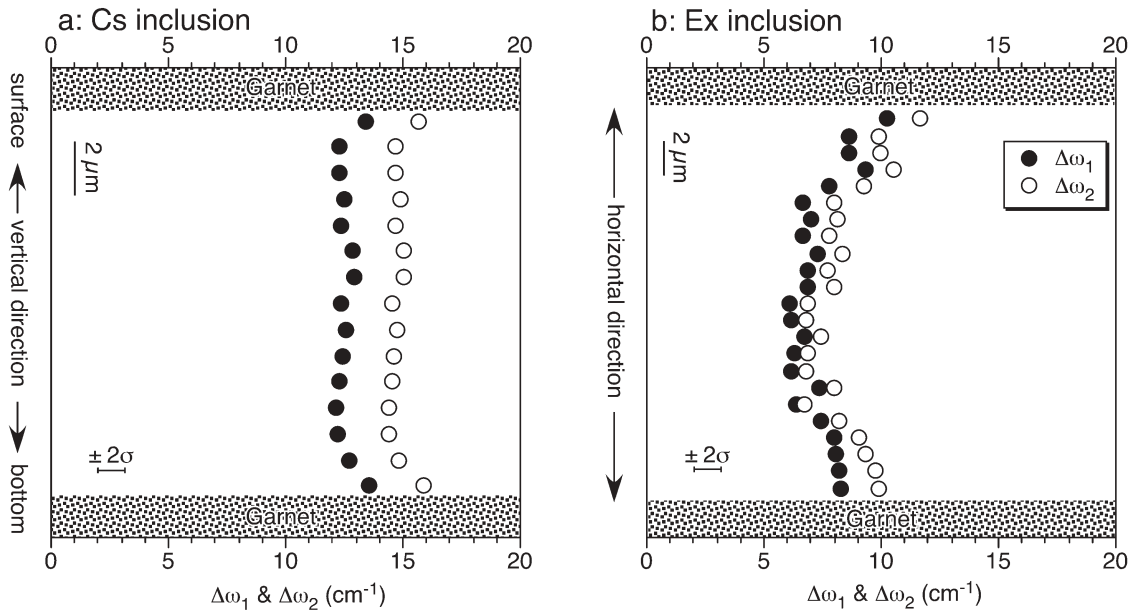

FIGURE 5. Step-scan analyses of the Cs quartz inclusion in garnet along vertical (depth) direction (**a**) and the Ex quartz inclusion in garnet along-horizontal direction on its surface (**b**) by the laser Raman microspectroscopy (GO01TT) at room temperature.

TABLE 1. Frequency shifts of Raman bands in spectra of quartz

Rock-types	Sample no.	Mode	Host	Frequency shift (in cm^{-1})			GS (μm)
				ω_1	ω_2	NOD	
Standard	α-quartz	// (0001)		259.0 (0.3)	77.8 (0.3)	41	
Quartz-eclogite facies				$\Delta\omega_1$	$\Delta\omega_2$	NA	
Qtz-rich eclogite	QE9601	Cs inc	Grt	9.8 (1.3)	11.2 (1.4)	27	12 (4)
		Ex inc	Grt	4.1 (0.9)	4.4 (0.9)	13	
		Fc inc	Grt	0.3 (0.4)	0.4 (0.5)	3	
		Cs inc	Ky	9.4 (1.8)	10.7 (2.4)	21	
		Cs inc	Omp	4.0 (2.3)	4.3 (2.4)	6	
		Cs inc	Ep	5.1 (1.8)	5.8 (1.6)	10	
		Matrix		–0.7 (0.7)	–0.4 (0.7)	3	
Qtz-rich eclogite	GO01TT	Cs inc	Grt	9.1 (2.2)	10.4 (2.7)	30	16 (7)
		Ex inc	Grt	5.6 (1.4)	6.2 (1.4)	18	
		Fc inc	Grt	1.7 (0.3)	2.2 (0.1)	2	
		Matrix		–0.1 (0.6)	0.1 (0.5)	19	
Qtz-poor eclogite	WK1304	Cs inc	Grt	8.9 (1.2)	10.0 (1.3)	19	15 (5)
		Ex inc	Grt	3.7 (1.2)	4.2 (1.1)	6	
		Fc inc	Grt	–0.3 (0.6)	0.0 (0.6)	3	
		Matrix		–0.3 (0.4)	–0.1 (0.4)	3	
Qtz-poor eclogite	WK1310	Cs inc	Grt	9.7 (1.1)	11.1 (1.1)	14	n.m.
		Ex inc	Grt	5.9 (1.3)	6.4 (1.6)	7	
		Fc inc	Grt	0.0 (0.2)	–0.2 (0.2)	2	
		Matrix	Grt	–0.2 (0.3)	–0.4 (0.4)	3	
Epidote-amphibolite facies							
Metapelite	AS1919	Cs inc	Grt	5.8 (1.8)	6.3 (1.9)	5	6 (2)
		Ex inc	Grt	2.4	3.4	1	
		Matrix		–0.2 (0.7)	–0.2 (0.7)	3	
Metapelite	AS2006	Cs inc	Grt	7.1 (0.8)	8.1 (1.0)	12	10 (4)
		Ex inc	Grt	3.8 (1.6)	4.6 (1.3)	8	
		Fc inc	Grt	0.2 (1.5)	0.2 (1.0)	2	
		Matrix		0.7 (0.4)	0.8 (0.4)	3	
Metachert	ST22F04b	Cs inc	Grt	7.0 (0.7)	8.0 (0.9)	42	8 (2)
		Ex inc	Grt	3.6 (1.2)	4.3 (1.3)	28	
		Fc inc	Grt	0.0 (0.7)	0.5 (0.6)	11	
		Matrix		–0.5 (0.3)	–0.3 (0.2)	5	
Metabasite	AS0305	Cs inc	Grt	4.5 (1.0)	5.1 (1.0)	13	n.m.
		Ex inc	Grt	2.5 (1.0)	2.7 (1.1)	7	
		Fc inc	Grt	–0.2	–0.2	1	
		Matrix		0.3 (0.7)	0.2 (0.8)	2	
Amphibolite facies							
Metapelite	104-9	Cs inc	Grt	0.8 (0.4)	1.0 (0.5)	6	19 (4)
		Ex inc	Grt	–0.2 (0.5)	0.0 (0.6)	6	
		Matrix		–0.4 (0.4)	–0.3 (0.3)	7	
Metapelite	148-2	Cs inc	Grt	1.6 (0.6)	1.7 (0.7)	12	20 (9)
		Ex inc	Grt	0.0 (0.3)	–0.1 (0.2)	6	
		Cs inc	St	–0.9 (0.6)	–0.7 (0.7)	10	
		Ex inc	St	–0.2 (0.8)	–0.1 (0.8)	10	
		Matrix		0.0 (0.3)	–0.2 (0.1)	4	

Notes: Grt = garnet; Ky = kyanite; Omp = omphacite; Ep = epidote; St = staurolite; NOD = Number of operating days; NA = Number of analyses; GS = grain size of inclusion; n.m. = not measured. Abbreviations for mode of quartz and parameters (ω_1, etc.) are described in the text. Number in parentheses indicates standard deviation (1σ level).

inclusions ($\Delta\omega_1 = -0.2 \pm 0.8$ cm^{-1} and $\Delta\omega_2 = -0.1 \pm 0.8$ cm^{-1}) and matrix quartz ($\Delta\omega_1 = 0.0 \pm 0.3$ cm^{-1} and $\Delta\omega_2 = -0.2 \pm 0.1$ cm^{-1}) (Table 1 and Fig. 9). The inverse relationships could indicate that the Cs inclusions in staurolite retain tensile stress (e.g., Ito et al. 1994; De Wolf 2003), and the relatively higher frequency shift of the Ex inclusion in staurolite implies release of the tensile stress in the process of making thin section.

Host crystals and Raman shift

The Cs quartz inclusions show systematic variations of the frequency shift depending on their host crystals (Fig. 10). In a quartz-rich eclogite (QE9601), the Cs quartz inclusions in garnet and kyanite have values similar to each other: $\Delta\omega_1 = 9.8 \pm 1.3$ cm^{-1} and $\Delta\omega_2 = 11.2 \pm 1.4$ cm^{-1} in garnet, and $\Delta\omega_1 = 9.4 \pm 1.8$ cm^{-1} and $\Delta\omega_2 = 10.7 \pm 2.4$ cm^{-1} in kyanite. The Cs inclusions in omphacite and epidote, on the other hand, have lower frequency shifts than those in garnet and kyanite: $\Delta\omega_1 = 4.0 \pm 2.3$ cm^{-1} and $\Delta\omega_2 = 4.3 \pm 2.4$ cm^{-1} in omphacite and $\Delta\omega_1 = 5.1 \pm 1.8$ cm^{-1} and $\Delta\omega_2 = 5.8 \pm 1.6$ cm^{-1} in epidote. The bulk modulus (κ_{298}) of garnet (166–175 GPa: Wang and Ji 2001) and kyanite (156–193 GPa: Comodi et al. 1997; Yang et al. 1997; Winkler et al. 2001a) are similar to each other, and are higher than those of omphacite (114–131 GPa: Bhagat et al. 1992; Pavese et al. 2001; Nishihara et al. 2003) and epidote (106–136 GPa: Ryzhova et al. 1966; Winkler et al. 2001b). In a metapelite of the amphibolite facies, the Cs quartz inclusions in staurolite with a low bulk modulus (124.6 GPa: Aleksandrov and Prodaivoda 1993) have lower frequency shifts than that in garnet as described in the previous section (Fig. 9). The positive correlations between the frequency shifts of Cs quartz inclusions and elastic parameters of their host crystals imply that the variations of Raman shift of quartz can be explained based on an elastic model as discussed below.

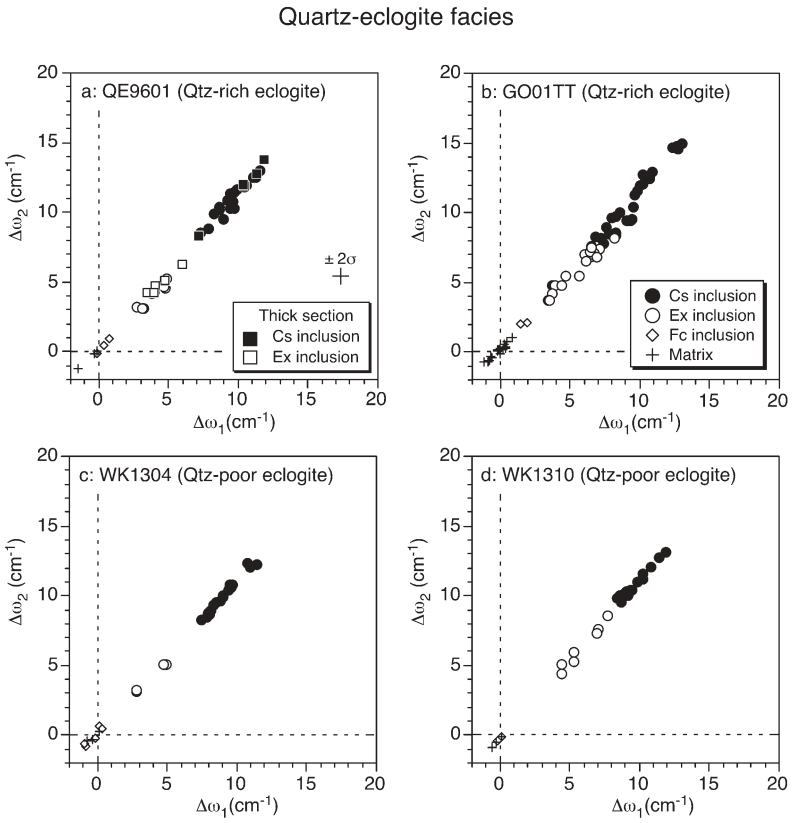

FIGURE 6. Correlation between the Raman frequency shifts ($\Delta\omega_1$ and $\Delta\omega_2$) of quartz and their modes of occurrence at room temperature for the quartz-eclogite-facies rocks from the eclogite unit of the Sanbagawa metamorphic belt. Squares indicate data from thicker section and other symbols show data from normal sections.

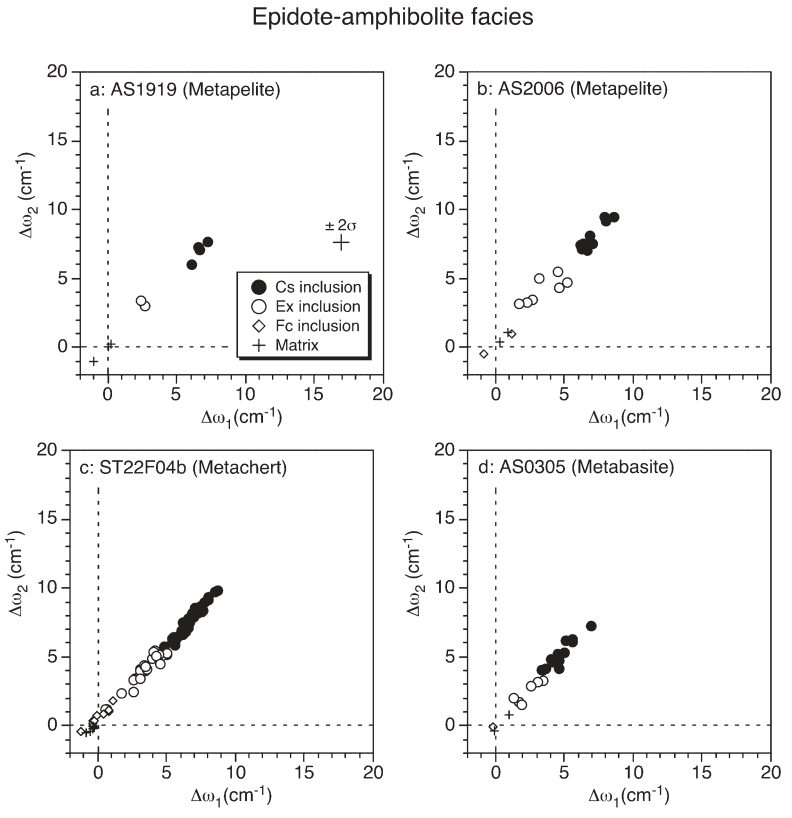

FIGURE 7. Correlation between the Raman frequency shifts ($\Delta\omega_1$ and $\Delta\omega_2$) of quartz and their modes of occurrence at room temperature for the epidote-amphibolite-facies rocks from the non-eclogite unit of the Sanbagawa metamorphic belt.

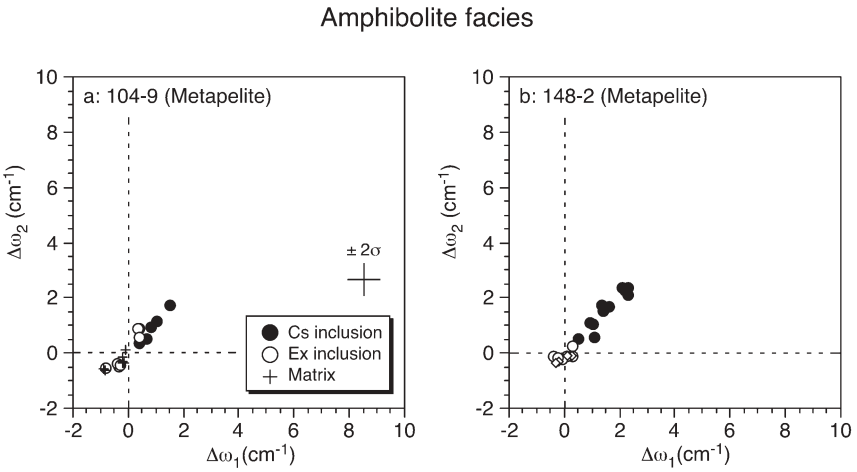

FIGURE 8. Correlation between the Raman frequency shifts ($\Delta\omega_1$ and $\Delta\omega_2$) of quartz and their modes of occurrence at room temperature for the amphibolite-facies rocks from the Altai metamorphic belt.

Raman barometry

The degree of Raman shift for quartz is intimately connected to its mode of occurrence (Figs. 6, 7, and 8) and physical properties of the host crystals (Figs. 9 and 10). Sobolev et al. (2000) reported that smaller coesite inclusions in diamond give a higher Raman shift than the larger ones. Wendt et al. (1993) numerically discussed a quantitative dependence between grain-size and confining pressure of α-quartz included in almandine-rich garnet. Accordingly, we discuss the relationships between the Raman frequency shifts of quartz inclusions and metamorphic *P-T* conditions using the data of Cs inclusions in garnet with regard to its grain size (Fig. 11). The frequency shifts of the Cs inclusions from the quartz-eclogite facies rocks show a weak negative correlation with inclusion size, and are 3.8–12.7 and 4.8–14.8 cm^{-1} for $\Delta\omega_1$ and $\Delta\omega_2$, respectively. The epidote-amphibolite- and amphibolite-facies samples do not show an obvious correlation between the frequency shifts and grain sizes, and have frequency shifts of $\Delta\omega_1$ = 5.2–8.5 and $\Delta\omega_2$ = 6.1–9.5 cm^{-1}, and $\Delta\omega_1$ = 0.7–2.3 and $\Delta\omega_2$ = 0.4–2.4 cm^{-1}, respectively, systematically lower than the quartz-eclogite facies rocks.

Raman spectra of quartz show a systematic pressure-dependent shift in series of experiments by Dean et al. (1982), Hemley (1987), Liu and Mernagh (1992), and Schmidt and Ziemann (2000). The systematic differences of frequency shifts shown in Figure 11 certainly reflect those of residual pressures retained by quartz. Applying the calibrations of Liu and Mernagh (1992) and Schmidt and Ziemann (2000), the maximum frequency shifts ($\Delta\omega_1$ and $\Delta\omega_2$) give residual pressures of 0.8–1.0, 0.4–0.6, and 0.1–0.2 GPa for the quartz-eclogite-, epidote-amphibolite- and amphibolite-facies samples, respectively (cf. Fig. 11 and Appendix 2 Fig. 2). The estimated residual pressures systematically increase in the ascending order of *P* and *P-T* conditions at the peak metamorphic stages.

Numerical simulation of internal pressures

Normal stresses (residual pressures) in and around a spherical inclusion have been formulated theoretically as a "spherical inclusion model" (e.g., Van der Molen 1981). Several varieties of the formulation have been applied to the problem of coesite retention in garnet from UHP metamorphic rocks (Gillet et al. 1984; Van der Molen and Van Roermund 1986; Nishiyama 1998). They have several features as summarized below.

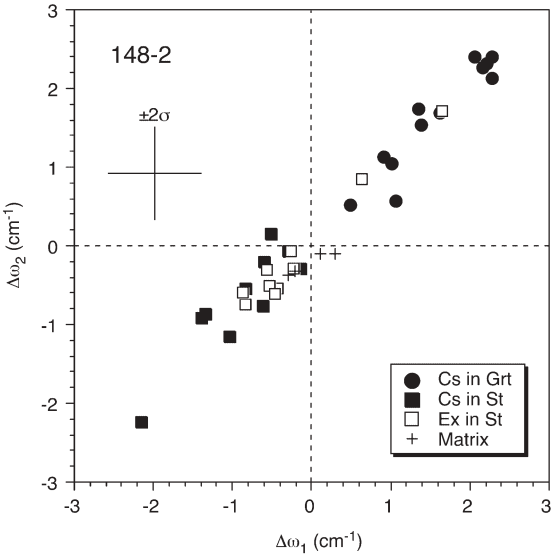

FIGURE 9. Comparison of the Raman frequency shifts ($\Delta\omega_1$ and $\Delta\omega_2$) of the Cs and Ex quartz inclusions in staurolite, Ex quartz inclusion in garnet, and matrix quartz of an amphibolite facies metapelite (148-2) at room temperature. Abbreviations are listed in Table 1.

The simplest model considers a spherical inclusion in an infinite isotropic medium with an external stress applied at infinity on the medium (Van der Molen 1981; Van der Molen and Van Roermund 1986). Elastic parameters of minerals are taken as constants and their dependence on temperature and pressure is neglected. Dependence of stresses on the grain size of the inclusion does not appear in this model.

The finite size model takes into account the grain size effects of both the inclusion and its host mineral on stresses in and around the inclusion (Gillet et al. 1984). The dependence of elastic parameters on temperature and pressure is also considered.

The three-shelled composite sphere model considers all spherical radii as parameters (Lee and Tromp 1995; Nishiyama 1998). The model can be extended to n-spherical shells (arbitrary number of shells). Elastic parameters are taken as constants. A volume change due to phase transition (or metamictization) is

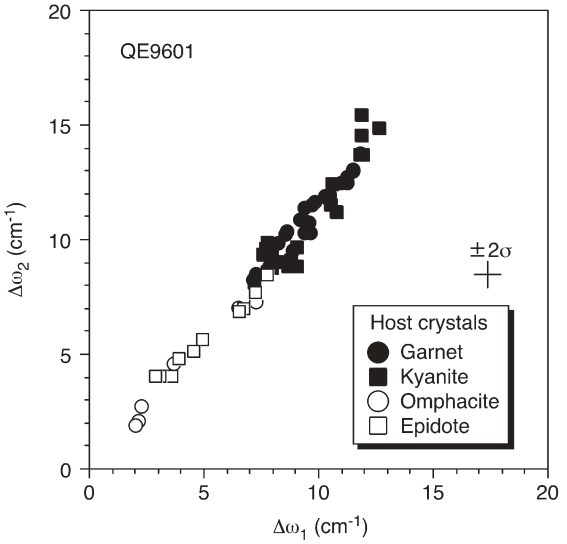

FIGURE 10. Comparison of the Raman frequency shifts ($\Delta\omega_1$ and $\Delta\omega_2$) of the Cs quartz included in garnet, kyanite, omphacite, and epidote of a quartz-rich eclogite (QE9601) at room temperature.

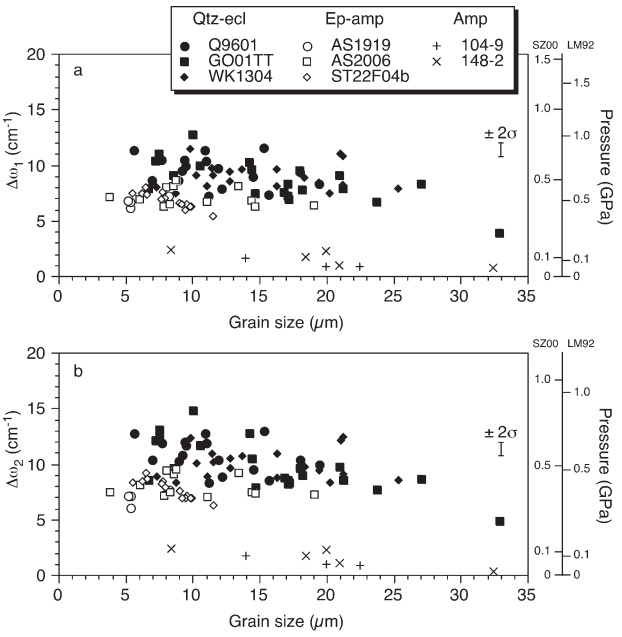

FIGURE 11. Correlations between the Raman frequency shifts ($\Delta\omega_1$ and $\Delta\omega_2$) of the Cs quartz inclusion in garnet and its grain size at room temperature. Grain size (**d**) was calculated as $d = \sqrt{a \times b}$, where *a* and *b* are, respectively, the major and minor axes of quartz inclusions approximated by an ellipsoid. Data for irregularly shaped quartz inclusions such as shown in Figures 3c and 3d are not shown in this figure. Abbreviations are Qtz-ecl = quartz-eclogite-facies sample; Ep-amp = epidote-amphibolite-facies sample; Amp = amphibolite-facies sample; LM92 = Liu and Mernagh (1992); SZ00 = Schmidt and Ziemann (2000). Pressure scale was calculated based on the pressure dependence of the Raman frequency shifts shown in Appendix 2 Figure 2.

considered, although thermal expansion is neglected.

From among these models we will adopt the simplest one because host garnets include several of inclusions that makes the exact application of the finite-size model difficult or even meaningless, and because all the inclusions in this study can be considered as originally included not as coesite but as quartz. According to Van der Molen (1981) the internal pressure P_{Qtz} (normal stress) of a spherical inclusion of quartz in garnet, which has undergone temperature change ΔT under the external pressure P_{Grt} on the garnet, can be written as

$$P_{Qtz} = \frac{\kappa_{Qtz}}{\kappa_{Grt}\left(3\kappa_{Qtz} + 4\mu_{Grt}\right)}\left\{P_{Grt}\left(3\kappa_{Grt} + 4\mu_{Grt}\right) - 4\kappa_{Grt}\mu_{Grt}\Delta T\Delta A\right\}$$

where κ denotes bulk modulus, μ is shear modulus, and ΔA stands for the difference of thermal expansion parameters between quartz and garnet defined as $\Delta A = A_{Grt} - A_{Qtz}$. Based on this equation, we calculated the internal pressures of quartz inclusions for four end-members of a garnet host: almandine, pyrope, grossular, and spessartine. Table 2 summarizes parameters used in our calculations. Elastic parameters are taken from Bass (1995) and Wang and Ji (2001), and thermal expansion parameters from Fei (1995). Our concept of the calculations is such that the system has experienced a temperature change from the peak temperature to 298 K under the external pressure, and that the inclusion will retain the internal pressure at atmospheric pressure after removal of the external pressure. Therefore, we used the magnitude of thermal expansion parameters at room temperature that will describe the misfit between the inclusion and the host causing the internal pressure at the final state (at room temperature and the external pressure P_{Grt}). Thermal expansion parameters at room temperature were calculated according to an equation given in Fei (1995, Table 1).

The calculated results of normal stress at standard conditions are listed in Table 3. The Sanbagawa eclogites (P_{peak} = 2.1–2.5 GPa and T_{peak} = 660–710 °C) show the internal pressure ranging from 0.68 to 0.85 GPa in the case of almandine, 0.78 to 0.95 GPa for pyrope, 0.38 to 0.49 GPa for grossular, and 0.71 to 0.88 GPa for spessartine. Because the host garnet in the studied samples is almandine-rich with moderate amounts of pyrope and grossular components, the calculated results for almandine and pyrope hosts are consistent with the residual pressure of 0.8–1.0 GPa measured by Raman spectroscopy (Fig. 11). As for the epidote-amphibolite-facies rocks in the non-eclogite unit (P_{peak} = 0.8–1.1 GPa and T_{peak}= 470–635 °C), the calculations give the internal pressure of 0.19–0.31 GPa for almandine, 0.26–0.38 GPa for pyrope, 0.08–0.15 GPa for grossular and 0.21–0.33 GPa for spessartine. The garnet in the metachert is spessartine-rich, with small or moderate amounts of almandine and grossular components, and that from metapelite and metabasite is a solid

TABLE 2. Bulk (κ) and shear (μ) moduli and thermal expansion parameter (*A*) at standard condition (10^{-4} GPa and 298 K)

Mineral	κ (GPa)	μ (GPa)	*A* (K^{-1})
Quartz	37.8*		2.38E-05‡
Almandine	175.1†	92.1†	1.57E-05‡
Pyrope	170.1†	90.2†	1.98E-05‡
Grossular	166.3†	98.1†	1.63E-05‡
Spessartine	171.8†	93.3†	1.71E-05‡

* Bass (1995).
† Wang and Ji (2001).
‡ Fei (1995).

TABLE 3. Numerical simulations of internal pressures of metamorphic quartz included in garnet at standard condition

Sanbagawa	Qtz-rich eclogite				Qtz-poor eclogite			
T_{peak} (°C)	665		710		660		690	
P_{peak} (GPa)	2.4	2.5	2.4	2.5	2.1	2.2	2.1	2.2
P_{Qtz} (GPa)								
in Alm	0.81	0.85	0.80	0.84	0.69	0.73	0.68	0.72
in Prp	0.90	0.95	0.90	0.94	0.78	0.82	0.78	0.82
in Grs	0.46	0.49	0.45	0.48	0.39	0.41	0.38	0.41
in Sps	0.84	0.88	0.83	0.87	0.72	0.76	0.71	0.75

Sanbagawa epidote-amphibolite facies rocks	Olig-biotite zone				Ab-biotite zone			
T_{peak} (°C)	585		635		470		590	
P_{peak} (GPa)	0.9	1.1	0.9	1.1	0.8	1.0	0.8	1.0
P_{Qtz} (GPa)								
in Alm	0.23	0.31	0.22	0.30	0.22	0.30	0.19	0.27
in Prp	0.30	0.38	0.30	0.38	0.27	0.36	0.26	0.34
in Grs	0.10	0.15	0.09	0.14	0.10	0.15	0.08	0.13
in Sps	0.25	0.33	0.24	0.32	0.23	0.31	0.21	0.29

Altai amphibolite facies rocks	470		570	
T_{peak} (°C)				
P_{peak} (GPa)	0.30	0.55	0.30	0.55
P_{Qtz} (GPa)				
in Alm	0.02	0.12	–0.01	0.09
in Prp	0.07	0.17	0.06	0.16
in Grs	–0.02	0.04	–0.04	0.02
in Sps	0.04	0.13	0.01	0.11

Notes: T_{peak} and P_{peak} = deduced peak metamorphic conditions; P_{Qtz} = estimated internal pressure at standard condition; Alm = almandine; Prp = pyrope; Grs = grossular; Sps = spessartine; Olig = oligoclase; Ab = albite.

solution of almandine, spessartine, and grossular. Incorporation of the grossular component will decrease the internal pressure drastically, but the effect may not be very large in the case of the Sanbagawa samples because the grossular contents are less than 30 mol%. The calculated results for the epidote-amphibolite-facies samples give an internal pressure 0.1–0.3 GPa less than the internal pressure measured by Raman spectroscopy (0.4–0.6 GPa, Fig. 11). Finally in the case of the Altai metapelites (P_{peak} = 0.30–0.55 GPa and T_{peak} = 470–570 °C), our calculation gives –0.01 to 0.12 GPa for almandine, 0.06–0.17 GPa for pyrope, –0.04 to 0.04 GPa for grossular, and 0.01 to 0.13 GPa for spessartine. Because the Altai garnets are almandine-rich with small amounts of grossular component (less than 8 mol%), the calculated results are consistent with the measured residual stresses of 0.1–0.2 GPa (Fig. 11). In summary, elastic modeling can predict the residual pressure around quartz inclusions in garnet, at least as a first approximation.

Use of residual pressure to identify high-metamorphic pressures

Because the residual pressures retained by quartz inclusions increase with increasing peak metamorphic pressures, they can be used to identify rocks that had undergone metamorphism under high pressures when other indicators are absent or have been destroyed. For example, systematic measurements of Raman spectra of quartz crystals implies that Cs quartz inclusions in garnet with $\Delta\omega_1 > 8.5 \pm 0.3$ and $\Delta\omega_2 > 9.5 \pm 03$ cm^{-1} at room temperature are inferred to be relics of quartz-eclogite-facies metamorphism in the Sanbagawa belt (Figs. 6, 7, and 11). Most of rocks in the Sanbagawa eclogite unit (Fig. 1b) were completely recrystallized during the exhumation and hydration stages, and thus have no phase diagnostic of eclogite-facies metamorphism such as omphacite. To find evidence for high-pressure metamorphism in such rocks, we applied Raman barometry to a metapelite

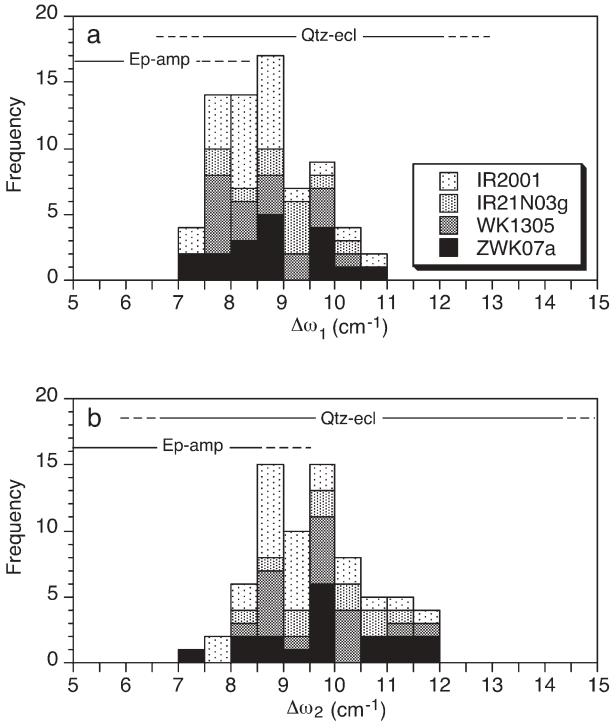

FIGURE 12. The Raman frequency shifts ($\Delta\omega_1$ and $\Delta\omega_2$) of the Cs quartz inclusions in garnet of metapelite (ZWK07a) and metabasites (IR2001, IR21N03g, and WK1305) from the inferred eclogite unit of the Sanbagawa belt (cf. Fig. 1b) at room temperature. These samples were completely recrystallized under the epidote-amphibolite-facies conditions, and preserve no phase diagnostic of the eclogite-facies stage. Abbreviations are listed in Figure 11.

(ZWK07a) and metabasites (IR2001, IR21N03g, and WK1305) in which there is no other evidence of eclogite-facies metamorphism. The metapelite (ZWK07a) contains quartz, garnet, paragonite, phengite, barroisite, chlorite, albite, and rutile as major matrix phases, and its equilibrium conditions at early high-pressure stage were estimated as 1.8 GPa and 520–550 °C based on the assemblage of chloritoid, barroisite, and paragonite included in garnet (Zaw Win Ko et al. 2005). The metabasites (IR2001, IR21N03g, and WK1305) consists mainly of barroisitic-taramitic amphibole, garnet, epidote, phengite, paragonite, plagioclase, quartz, and rutile. The Cs inclusions in garnet record high $\Delta\omega_1$ and $\Delta\omega_2$ values, i.e., 10.8 and 11.9 cm^{-1} in ZWK07a, 10.6 and 11.7 cm^{-1} in IR2001, 10.3 and 11.4 cm^{-1} in IR21N03g, and 10.3 and 11.6 cm^{-1} in WK1305, respectively (Fig. 12). Thus, it is almost certain that the four samples have experienced quartz-eclogite-facies metamorphism, demonstrating that Raman spectrometry is a powerful and useful tool for recognizing signatures of higher-pressure conditions in metamorphic rocks recrystallized during the subsequent exhumation and hydration.

Acknowledgments

We are deeply indebted to S. Dunn (Mount Holyoke College), H. Kagi (University of Tokyo), I.-M. Chou (U.S. Geological Survey), and E.S. Grew (University of Maine) for their careful reading and constructive suggestions, which led to significant improvements in the manuscript, and appreciate Y. Hirahara (Nagoya University), S. Wallis (Nagoya University), and two anonymous reviewers for commenting on the earlier versions of this manuscript. We also thank C.Q. Zheng (Jilin University) for giving the loan of the Altai samples, and to R. Harui (Thermo Fisher Scientific K.K.) for giving approval to quote the unpublished data. This study was supported financially in part by Grant-Aid for Scientific Research from JSPS (M.E., 14540448 and 18340172).

References cited

Aleksandrov, K.S. and Prodaivoda, G.T. (1993) Elastic properties of minerals. Crystallography Reports, 38, 214–234.

Aoya, M. (2001) *P-T-D* path of eclogite from the Sambagawa belt deduced from combination of petrological and microstructural analyses. Journal of Petrology, 42, 1225–1248.

Banno, S. and Nakajima, T. (1992) Metamorphic belts of Japanese islands. Annual Review of Earth and Planetary Sciences, 20, 159–179.

Banno, S., Yokoyama, K., Iwata, O., and Terashima, S. (1976) Genesis of epidote amphibolite masses in the Sanbagawa metamorphic belt of central Shikoku. Journal of Geological Society of Japan, 82, 199–210 (in Japanese with English abstract).

Banno, Y. (2000) Intermediate high-pressure exhumation of the northern segment of the Sanbagawa belt, Saruta-gawa area, central Shikoku, Japan. Lithos, 50, 289–303.

Bass, J.D. (1995) Elasticity of minerals, glasses, and metals. In T.J. Ahrens, Ed., Mineral physics and crystallography: A handbook of physical constants, 2, p. 45–63. American Geophysical Union, Washington, D.C.

Bhagat, S.S., Bass, J.D., and Smyth, J.R. (1992) Single-crystal elastic properties of omphacite-*C*2/*c* by Brillouin spectroscopy. Journal of Geophysical Research, B, Solid Earth and Planets, 97, 6843–6848.

Boyer, H., Smith, D.C., Chopin, C., and Lasnier, B. (1985) Raman microprobe (RMP) determinations of natural and synthetic coesite. Physics and Chemistry of Minerals, 12, 45–48.

Comodi, P., Zanazzi, P.F., Poli, S., and Schmidt, M.W. (1997) High-pressure behavior of kyanite: Compressibility and structural deformations. American Mineralogist, 82, 452–459.

De Wolf, I. (2003) Raman spectroscopy: about chips and stress. Spectroscopy Europe, 15, 6–13.

Dean, K.J., Sherman, W.F., and Wilkinson, G.R. (1982) Temperature and pressure dependence of the Raman active modes of vibration of α-quartz. Spectrochimica Acta A, 38, 1105–1108.

Enami, M. (1983) Petrology of pelitic schists in the oligoclase-biotite zone of the Sanbagawa metamorphic terrain, Japan: phase equilibria in the highest grade zone of a high-pressure intermediate type of metamorphic belt. Journal of Metamorphic Geology, 1, 141–161.

Enami, M., Wallis, S.R., and Banno, Y. (1994) Paragenesis of sodic pyroxene-bearing quartz schists: implications for the *P-T* history of the Sanbagawa belt. Contributions to Mineralogy and Petrology, 116, 182–198.

Etchepare, J., Merian, M., and Smetankine, L. (1974) Vibrational normal modes of SiO_2. I. α and β quartz. Journal of Chemical Physics, 60, 1873–1876.

Fei, Y. (1995) Thermal expansion. In T.J. Ahrens, Ed., Mineral Physics and Crystallography: A Handbook of Physical Constants, 2, p. 29–44. American Geophysical Union, Washington, D.C.

Fukura, S., Mizukami, T., Odake, S., and Kagi, H. (2006) Factors Determining the Stability, Resolution, and Precision of a Conventional Raman Spectrometer. Applied Spectroscopy, 60, 946–950.

Gillet, P., Ingrin, J., and Chopin, C. (1984) Coesite in subducted continental crust: *P-T* history deduced from an elastic model. Earth and Planetary Science Letters, 70, 426–436.

Gillet, P., Sautter, V., Harris, J., Reynard, B., Harte, B., and Kunz, M. (2002) Raman spectroscopic study of garnet inclusions in diamonds from the mantle transition zone. America Mineralogist, 87, 312–317.

Hemley, R.J. (1987) Pressure dependence of Raman spectra of SiO_2 polymorphs; α-quartz, coesite, and stishovite. In H. Manghnani Murli and Y. Syono, Eds., High-pressure research in mineral physics, 39, p. 347–359. American Geophysical Union, Washington, D.C.

Higashino, T. (1990) The higher-grade metamorphic zonation of the Sambagawa metamorphic belt in central Shikoku, Japan. Journal of Metamorphic Geology, 8, 413–423.

Holland, T.J.B. and Powell, R. (1998) An internally consistent thermodynamic data set for phases of petrological interest. Journal of Metamorphic Geology, 16, 309–343.

Ito, T., Azuma, H., and Noda, S. (1994) Stress measurements in silicon substrates with $TiSi_2$ patterns using Raman microprobe. Japanese Journal of Applied Physics, 33, 171–177.

Izraeli, E.S., Harris, J.W., and Navon, O. (1999) Raman barometry of diamond formation. Earth and Planetary Science Letters, 173, 351–360.

Kretz, R. (1983) Symbols for rock-forming minerals. American Mineralogist, 68, 277–279.

Krogh Ravna, E.J. and Terry, M.P. (2004) Geothermobarometry of UHP and HP eclogites and schists; an evaluation of equilibria among garnet-clinopyroxene-kyanite-phengite-coesite/quartz. Journal of Metamorphic Geology, 22, 579–592.

Kurata, H. and Banno, S. (1974) Low-grade progressive metamorphism of pelitic schists of the Sazare area, Sanbagawa metamorphic terrain in central Shikoku, Japan. Journal of Petrology, 15, 361–382.

Lee, J.K.W. and Tromp, J. (1995) Self-induced fracture generation in zircon. Journal of Geophysical Research B: Solid Earth and Planets, 100, 17753–17770.

Liu, J., Ye, K., Maruyama, S., Cong, B., and Fan, H. (2001) Mineral inclusions in zircon from gneisses in the ultrahigh-pressure zone of the Dabie Mountains, China. Journal of Geology, 109, 523–535.

Liu, L.G. and Mernagh, T.P. (1992) High-pressure Raman study of the α-quartz forms of SiO_2 and GeO_2 at room temperature. High Temperatures-High Pressures, 24, 13–21.

Nishihara, Y., Takahashi, E., Matsukage, K., and Kikegawa, T. (2003) Thermal equation of state of omphacite. American Mineralogist, 88, 80–86.

Nishiyama, T. (1998) Kinetic modeling of the coesite-quartz transition in an elastic field and its implication for the exhumation of ultrahigh-pressure metamorphic rocks. The Island Arc, 7, 70–81.

Ota, T., Terabayashi, M., and Katayama, I. (2004) Thermobaric structure and metamorphic evolution of the Iratsu eclogite body in the Sanbagawa belt, central Shikoku, Japan. Lithos, 73, 95–126.

Otsuki, M. and Banno, S. (1990) Prograde and retrograde metamorphism of hematite-bearing basic schists in the Sanbagawa belt in central Shikoku. Journal of Metamorphic Geology, 8, 425–439.

Parkinson, C.D. (2000) Coesite inclusions and prograde compositional zonation of garnet in whiteschist of the HP-UHPM Kokchetav massif, Kazakhstan: A record of progressive UHP metamorphism. Lithos, 52, 215–233.

Parkinson, C.D. and Katayama, I. (1999) Present-day ultrahigh-pressure conditions of coesite inclusions in zircon and garnet: Evidence from laser Raman microspectroscopy. Geology, 27, 979–982.

Pattison, D.R.M. (1992) Stability of andalusite and sillimanite and the Al_2SiO_5 triple point; constraints from the Ballachulish aureole, Scotland. Journal of Geology, 100, 423–446.

Pavese, A., Diella, V., Levy, D., and Hanfland, M. (2001) Synchrotron X-ray powder diffraction study of natural *P*2/*n*-omphacites at high-pressure conditions. Physics and Chemistry of Minerals, 28, 9–16.

Ryzhova, T.V., Aleksandrov, K.S., and Korobkova, V.M. (1966) The elastic properties of rock-forming minerals; V, Additional data on silicates. Physics of the Solid Earth, 2, 63–65.

Schmidt, C. and Ziemann, M.A. (2000) In-situ Raman spectroscopy of quartz; a pressure sensor for hydrothermal diamond-anvil cell experiments at elevated temperatures. American Mineralogist, 85, 1725–1734.

Sharma, S.K., Mammone, J.F., and Nicol, M.F. (1981) Raman investigation of ring configurations in vitreous silica. Nature, 292, 140–141.

Sobolev, N.V. and Shatsky, V.S. (1990) Diamond inclusions in garnets from metamorphic rocks; a new environment for diamond formation. Nature, 343, 742–746.

Sobolev, N.V., Shatsky, V.S., Vavilov, M.A., and Goryaynov, S.V. (1995) Zircon in high-pressure metamorphic rocks in folded regions as a unique container of inclusions of diamond, coesite, and coexisting minerals. Transactions of the

Russian Academy of Sciences. Earth Science Sections, 336, 79–85.
Sobolev, N.V., Fursenko, B.A., Goryainov, S.V., Shu, J., Hemley, R.J., Mao, H.K., and Boyd, F.R. (2000) Fossilized high pressure from the Earth's deep interior: the coesite-in-diamond barometer. Proceedings of National Academy of Sciences, USA, 97, 11875–11879.
Tabata, H., Maruyama, S., and Shi, Z. (1998) Metamorphic zoning and thermal structure of the Dabie ultrahigh-pressure-high-pressure terrane, central China. The Island Arc, 7, 142–158.
Takasu, A. (1989) *P-T* histories of peridotite and amphibolite tectonic blocks in the Sambagawa metamorphic belt, Japan. In J.S. Daly, R.A. Cliff, and B.W.D. Yardley, Eds., The Evolution of Metamorphic Belts, 43, p. 533–538. Blackwell Scientific Publications, Oxford.
Takasu, A., Wallis, S.R., Banno, S., and Dallmeyer, R.D. (1994) Evolution of the Sambagawa metamorphic belt, Japan. Lithos, 33, 119–133.
Tsujimori, T., Tanaka, C., Sakurai, T., Matsumoto, M., Miyagi, Y., Mizukami, T., Kugimiya, Y., and Aoya, M. (2000) Illustrated introduction to eclogite in Japan. Bulletin of Research Institute of Natural Sciences, Okayama University of Science, 26, 19–40.
Van der Molen, I. (1981) The shift of the α-β transition temperature of quartz associated with the thermal expansion of granite at high pressure. Tectonophysics, 73, 323–342.
Van der Molen, I. and Van Roermund, H.L.M. (1986) The pressure path of solid inclusions in minerals: the retention of coesite inclusions during uplift. Lithos, 19, 317–324.
Wallis, S. and Aoya, M. (2000) A re-evaluation of eclogite facies metamorphism in SW Japan: Proposal for an eclogite nappe. Journal of Metamorphic Geology, 18, 653–664.
Wallis, S., Takasu, A., Enami, M., and Tsujimori, T. (2000) Eclogite and related metamorphism in the Sanbagawa belt, Southwest Japan. Bulletin of Research Institute of Natural Sciences, Okayama University of Science, 26, 3–17.
Wang, A., Jolliff, B.L., and Haskin, L.A. (1999) Raman spectroscopic characterization of a Martian SNC meteorite; Zagami. Journal of Geophysical Research, E, Planets, 104, 8509–8519.
Wang, Z. and Ji, S. (2001) Elasticity of six polycrystalline silicate garnets at pressure up to 3.0 GPa. American Mineralogist, 86, 1209–1218.
Wendt, A.S., D'Arco, P., Goffé, B., and Oberhänsli, R. (1993) Radial cracks around α-quartz inclusions in almandine; constraints on the metamorphic history of the Oman mountains. Earth and Planetary Science Letters, 114, 449–461.
Windley, B.F., Kröner, A., Guo, J., Qu, G., Li, Y., and Zhang, C. (2002) Neoproterozoic to Paleozoic geology of the Altai orogen, NW China: New Zircon age data and tectonic evolution. Journal of Geology, 110, 719–737.
Winkler, B., Hytha, M., Warren, M.C., Milman, V., Gale, J.D., and Schreuer, J. (2001a) Calculation of the elastic constants of the Al_2SiO_5 polymorphs andalusite, sillimanite and kyanite. Zeitschrift für Kristallographie, 216, 67–70.
Winkler, B., Milman, V., and Nobes, R.H. (2001b) A theoretical investigation of the relative stabilities of Fe-free clinozoisite and orthozoisite. Physics and Chemistry of Minerals, 28, 471–474.
Yamamoto, J., Kagi, H., Kaneoka, I., Lai, Y., Prikhod'ko, V.S., and Arai, S. (2002) Fossil pressures of fluid inclusions in mantle xenoliths exhibiting rheology of mantle minerals; implications for the geobarometry of mantle minerals using micro-Raman spectroscopy. Earth and Planetary Science Letters, 198, 511–519.
Yang, H., Downs, R.T., Finger, L.W., Hazen, R.M., and Prewitt, C.T. (1997) Compressibility and crystal structure of kyanite, Al_2SiO_5, at high pressure. American Mineralogist, 82, 467–474.
Ye, K., Yao, Y., Katayama, I., Cong, B., Wang, Q., and Maruyama, S. (2000) Large areal extent of ultrahigh pressure-metamorphism in the Sulu UHP terrain of Eastern China: new implications from coesite and omphacite inclusions in zircon of granitic gneiss. Lithos, 52, 157–164.
Ye, K., Liou, J.G., Cong, B., and Maruyama, S. (2001) Overpressures induced by coesite-quartz transition in zircon. American Mineralogist, 86, 1151–1155.
Zaw Win Ko, Enami, M., and Aoya, M. (2005) Chloritoid and barroisite-bearing pelitic schists from the eclogite unit in the Besshi district, Sanbagawa metamorphic belt. Lithos, 81, 79–100.
Zedgenizov, D.A., Kagi, H., Shatsky, V.S., and Sobolev, N.V. (2004) Carbonatitic melts in cuboid diamonds from Udachnaya kimberlite pipe, Yakutia; evidence from vibrational spectroscopy. Mineralogical Magazine, 68, 61–73.
Zheng, C.Q., Xu, X.C., Enami, M., and Kato, T. (2005) Monazite ages and geological implications of andalusite-sillimanite type metamorphic belt in Aletai, Xinjiang, China. Global Geology, 24, 236–242 (in Chinese with English abstract).

Manuscript received August 30, 2006
Manuscript accepted March 9, 2007
Manuscript handled by Edward Grew

Appendix 1: Petrology of samples studied

Representative mineral compositions are listed in Appendix Table 1.

Sanbagawa quartz eclogite

Sample QE9601 is composed mainly of garnet ($Alm_{45–60}Prp_{21–39}Sps_{1–3}Grs_{11–25}$), omphacite ($Jd_{44–48}Aug_{45–54}Aeg_{0–10}$), phengite (Si = 3.27–3.35 per formula unit: pfu for O = 11), kyanite, epidote [$Y_{Fe} = Fe^{3+}/(Al + Cr + Fe^{3+}) = 0.17–0.20$], and quartz, with small amounts of rutile, apatite, and zircon. [Abbreviations of end-members follow Kretz (1983) other than Aeg (aegirine).] Rutile needles (1–2 × 10–30 μm) have exsolved from the core part of zoned garnet. Glaucophane (Al = 1.50–1.61 pfu and Na = 1.81–1.82 pfu for O = 23) is included in garnet. Omphacite is rimmed by secondary symplectitic aggregates of barroisite (Si = 6.57–7.61 pfu and Ca = 0.63–1.48 pfu) + albite ($An_{5–9}$), whereas kyanite is replaced by fine-grained mixtures of phengite and paragonite. Secondary titanite rims matrix rutile. It is not clear whether paragonite was stable at the peak eclogite stage: it occurs both as inclusions in garnet and as isolated grains in the matrix.

Sample GO01TT has constituent minerals and mineral chemistries similar to those of QE9601, except that kyanite is absent.

Sample WK1304 consists mainly of garnet ($Alm_{43–55}Prp_{8–16}Sps_{1–12}Grs_{29–37}$), omphacite ($Jd_{34–44}Aug_{50–66}Aeg_{0–6}$), phengite (Si = 3.29–3.32 pfu), epidote (Y_{Fe} = 0.12–0.16), and quartz with accessory rutile, titanite and apatite. Pargasite-hornblende/barroisite (Si = 6.26–6.68 pfu, Ca = 1.28–1.65 pfu) is included in garnet. Slightly Si-richer amphiboles occur as independent grains (Si = 6.73–7.46 pfu and Ca = 1.34–1.77 pfu) and symplectitic aggregates (Si = 6.88–7.49 pfu and Ca = 1.60–1.76 pfu) with albite ($An_{1–3}$) in the matrix.

Sample WK1310 is composed mainly of garnet ($Alm_{52–60}Prp_{9–17}Sps_{2–7}Grs_{23–29}$), omphacite ($Jd_{39–47}Aug_{47–56}Aeg_{0–6}$), phengite (Si = 3.29–3.32 pfu), epidote (Y_{Fe} = 0.14–0.18), and quartz with accessory rutile and apatite. Barroisitic amphibole (Si = 6.68–7.15 pfu and Ca = 1.05–1.41 pfu) occurs as inclusions in garnet and omphacite. Isolated amphibole grains in the matrix have pargasitic-katophoritic compositions (Si = 6.03–6.76 pfu and Ca = 1.19–1.64 pfu) and symplectitic amphibole aggregates with albite ($An_{1–9}$) have edenitic-actinolitic compositions (Si = 6.79–7.30 pfu and Ca = 1.66–1.73 pfu). Secondary titanite rims rutile.

Sanbagawa epidote-amphibolite-facies rocks

Metapelite (AS2006) consists of garnet ($Alm_{39–70}Prp_{1–9}Sps_{1–41}Grs_{19–33}$), biotite [$X_{Mg} = Mg/(Mg + Fe) = 0.48–0.50$, TiO_2 = 1.3–1.4 wt%], chlorite (X_{Mg} = 0.47–0.55), phengite (Si = 3.24–2.38 pfu), epidote, pargasite/hornblende (Si = 6.41–6.98 pfu and Ca = 1.51–1.72 pfu), albite ($An_{1–3}$), titanite, rutile, apatite and fully ordered graphite.

Sample AS1919 has constituent minerals and mineral chemistries similar to those of AS2006, except that amphibole and biotite are absent and tourmaline is present.

Metachert (ST22F04b) is composed predominantly of quartz with subordinate amounts of garnet ($Alm_{9–23}Prp_{3–9}Sps_{55–75}Grs_{13–15}$)], winchite (Si = 7.18–7.37 pfu and Ca = 0.65–0.93 pfu), epidote (Y_{Fe} = 0.28–0.29)/piemontite, phengite (Si = 3.27–3.37 pfu) and albite and accessory ilmenohematite and apatite.

Metabasite (AS0305) is mainly composed of taramite (Si = 6.21–6.49 pfu and Ca = 1.32–1.49 pfu), garnet ($Alm_{57–71}$

APPENDIX TABLE 1. Representative analyses of major constituent minerals

	Quartz-eclogite facies						Epidote-amphibolite facies							Amphibolite facies			
	Qtz-rich eclogite QE9601			Qtz-poor eclogite WK1310			Metapelite AS2006				Metabasite AS0305			Metapelite 148-2			
	Grt	Cpx	Ms	Grt	Cpx	Ms	Grt	Bt	Amp	Chl	Grt	Amp	Ms	Grt	Bt	Ms	Pl
SiO_2	39.8	55.0	49.1	38.8	55.4	49.1	37.4	37.2	42.7	26.1	37.8	42.2	46.5	37.5	36.8	46.1	56.5
TiO_2	0.01	0.21	0.45	0.19	0.14	0.36	0.04	1.41	0.41	0.06	0.04	0.47	0.66	0.00	1.53	0.49	0.00
Al_2O_3	22.5	11.1	28.4	21.9	10.6	29.8	21.1	15.9	15.0	20.9	20.7	15.3	31.3	21.3	19.0	34.7	27.4
Cr_2O_3	0.02	0.00	0.03	0.01	0.00	0.00	n.a.	n.a.	n.a.	n.a.	n.a.	n.a.	n.a.	n.a.	n.a.	n.a.	n.a.
FeO*	22.9	6.47	2.69	25.4	6.54	2.60	30.0	19.9	16.3	23.9	31.3	17.2	3.81	27.2	14.1	1.56	0.28
MnO	0.41	0.03	0.00	1.48	0.20	0.02	0.48	0.09	0.05	0.00	1.14	0.07	0.00	7.80	0.15	0.00	0.00
MgO	9.28	7.30	3.02	4.43	7.39	2.72	2.20	11.1	8.24	16.1	3.53	8.86	1.64	3.80	13.5	0.68	0.02
BaO	n.a.	n.a.	0.11	n.a.	n.a.	n.a.	n.a.	n.a.	n.a.	n.a.	n.a.	n.a.	0.68	n.a.	n.a.	n.a.	n.a.
CaO	6.02	11.9	0.02	8.77	12.3	0.01	7.95	0.00	9.87	0.01	5.67	9.42	0.01	2.67	0.00	0.02	9.51
Na_2O	n.a.	7.26	1.01	n.a.	7.07	1.06	n.a.	0.07	3.19	0.00	n.a.	3.03	1.61	n.a.	0.35	1.30	6.30
K_2O	n.a.	0.00	9.98	n.a.	0.00	9.81	n.a.	9.55	0.48	0.00	n.a.	0.45	8.78	n.a.	9.07	9.54	0.04
Total	100.94	99.27	94.81	100.98	99.64	95.48	99.17	95.22	96.24	87.11	100.18	97.00	94.99	100.27	94.50	94.39	100.07

* Total iron as FeO. Abbreviations are Qtz = quartz; Grt = garnet; Cpx = clinopyroxene; Ms = white mica; Bt = biotite; Amp = amphibole; Chl = chlorite; Pl = plagioclase; n.a. = not analyzed.

$Prp_{4–14}Sps_{1–12}Grs_{14–29}$), epidote ($Y_{Fe}$ = 0.27–0.28), muscovite (Si = 3.13–3.26 pfu), oligoclase, quartz, ilmenite, dolomite/calcite, rutile and apatite. Titanite occurs as inclusions in garnet. Secondary chlorite (X_{Mg} = 0.51) partly replaces garnet.

Altai amphibolite facies rocks

Sample 104–9 consists mainly of garnet ($Alm_{64–71}Prp_{5–12}Sps_{10–21}Grs_{6–8}$), biotite ($X_{Mg}$ = 0.51–0.54 and TiO_2 = 1.3–1.6 wt%), muscovite (Si = 3.06–3.13 pfu), staurolite (X_{Mg} = 0.14–0.18 and ZnO = 0.23–0.41 wt%), andalusite, chlorite (X_{Mg} = 0.53–0.55) and quartz with accessory ilmenite and apatite.

Sample 148-2 is composed mainly of garnet ($Alm_{60–63}Prp_{12–15}Sps_{17–20}Grs_{5–8}$), biotite ($X_{Mg}$ = 0.62–0.63 and TiO_2 = 1.3–1.6 wt%), muscovite (Si = 3.07–3.12 pfu), staurolite (X_{Mg} = 0.25–0.26 and ZnO = 0.10–0.22 wt%), kyanite, chlorite, plagioclase ($An_{36–55}$) and quartz with accessory ilmenite and apatite.

APPENDIX 2: BASIC DATA OF RAMAN SHIFT OF α-QUARTZ

The stability of Raman spectra was verified by continuous measurement of α-quartz standard over five hours (Appendix 2 Fig. 1). The frequency shifts of the 464 and 128 cm^{-1} bands gradually decreased by a small amount during the first hour of measurement, and then were fairly constant over the remaining four hours. The 205 cm^{-1} band has a broader peak width and consequently a larger standard deviation (±0.3 cm^{-1} for 1σ level) of the frequency shift than the 464 and 128 cm^{-1} bands (±0.03–0.04 cm^{-1}). Fukura et al. (2006) carefully considered factors determining the stability, resolution, and precision of a conventional Raman spectrometer in their laboratory, and reported that a change of 0.4 °C in room temperature causes peak positions of ruby fluorescence spectrum to shift by 0.052 cm^{-1}. In our case, variation in room temperature of 0.7 °C seems to have but a minor effect on the frequency shifts considering the analytical precision of 0.03–0.3 cm^{-1}.

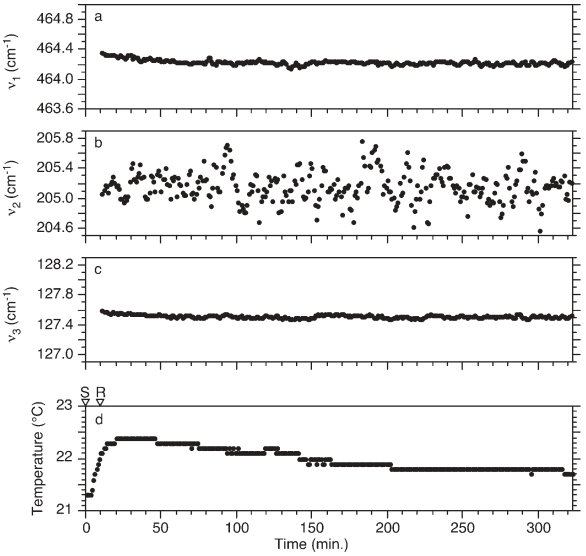

APPENDIX 2 FIGURE 1. Changes in the Raman frequency shifts of (**a**) 464, (**b**) 205, and (**c**) 128 cm^{-1} bands and (**d**) room temperature with time. S = Start-up of the Raman spectral instrument; R = Completion of CCD detector cooling and Raman measurement start.

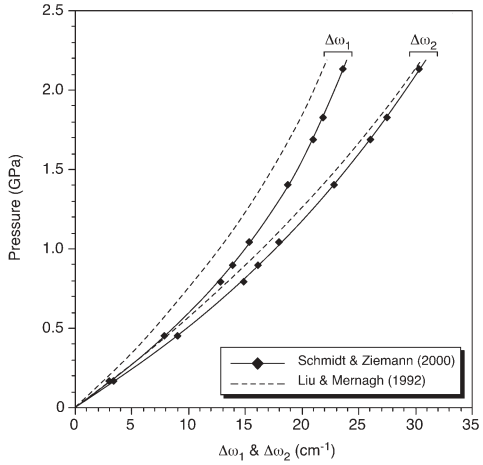

APPENDIX 2 FIGURE 2. Frequency shifts ($\Delta\omega_1$ and $\Delta\omega_2$) in the Raman spectrum of α-quartz as a function of pressure at room temperature. Data are from Schmidt and Ziemann (2000) = solid lines and filled diamonds; Liu and Mernagh (1992) = dashed line.